International Journal of Engineering

Journal Homepage: www.ije.ir

Microstructure and Corrosion Behavior of Al-Cu-Fe Quasi-crystalline Coated Ti-6Al-4V Alloy

M. Abaei, M. R. Rahimipour*, M. Farvizi*, M. J. Eshraghi

Department of Ceramic, Materials, and Energy Research Center, Karaj, Iran

P A P E R I N F O

Paper history:
Received 30 May 2023
Received in revised form 12 July 2023
Accepted 14 July 2023

Keywords:
$Al_{65}Cu_{20}Fe_{15}$ Phase
Corrosion Resistance
Quasicrystals
Thin Film
Ti-6Al-4V Alloy

A B S T R A C T

Different industries, including aerospace, marine, and automotive, widely use titanium alloys such as Ti-6Al-4V. Although, this alloy has excellent properties; it is highly susceptible to corrosion and has low thermal stability and tribological characteristics, limiting its application. In this research, after preparing the $Al_{62.5}Cu_{25}Fe_{12.5}$ quasi-crystalline (QC) powder mixture and appropriate target, the magnetron sputtering method was employed to deposit the QC coating on the Ti-6Al-4V substrate. The powder mixture and AlCuFe thin films were annealed at 700^0C for 2 h. The scanning electron microscope (SEM) analysis and X-ray diffraction (XRD) methods were used to investigate the microstructure and morphology of mixed powders and Al-Cu-Fe QC coatings. NaCl solution (3.5 wt.%) was utilized to conduct the electrochemical measurements. Al-Cu-Fe thin layer deposited on the Ti-6Al-4V alloy surface without any cracks. The XRD patterns related to the annealed powders and the coating after heat treatment indicated the presence of Cu_3Al, $AlFe_3$, and quasi-crystalline ternary phases of $Al_{65}Cu_{20}Fe_{15}$, Al_3Fe, $AlTi_2$, and $Al_{65}Cu_{20}Fe_{15}$ phases, respectively. Based on the polarization test results, the annealed coating at 700°C showed better electrochemical behavior than the Ti-6Al-4V substrate.

***doi**: 10.5829/ije.2023.36.10a.13*

1. INTRODUCTION

Titanium and its alloys are extensively employed in automotive, biomedical, and aerospace industries due to their unique properties including biocompatibility, high strength-to-weight ratio, and low modulus of elasticity. In contempt of the different pleasant assets of Ti–6Al–4V alloy, the operation of this alloy is restricted, especially when it comes to tribological applications characteristics [1]. Although Ti-6Al-4V alloy has several unique characteristics, its durability in engineering is restricted because they are not hard enough and also highly sensitive to corrosion.

Quasicrystals not only show different structural features, such as the absence of translational symmetry that is representative of non-crystalline materials but also represent the feature of crystalline materials (e.g., generating sharp peaks in XRD). Quasicrystalline materials are appropriate for many practical applications due to their unique characteristics, including significant hardness, and notable resistance to corrosion. Previous studies [2] have shown that the developing of mixed quasi-crystalline (QC) coatings can enhance the titanium alloy's wear resistance (grade five). The performance of wear resistance for the Al-Cu-5Fe coating was 2.8 times that of the substrate. Although QCs have limited applications as structural materials due to their brittle nature, their distinctive characteristics raise the possibility of applications as functional materials in several fields such as a catalytic agent to produce hydrogen [3,4].

According to the type of coating, the methods of obtaining quasicrystalline coatings are divided into two groups (including powder and film coatings). While powder coatings are made using thermal-gaseous and electrochemical procedures, film coatings are obtained through various physical procedures, including chemical vapor deposition (CVD). Plasma spray and High-

*Corresponding Authors Email: m-rahimi@merc.ac.ir (M. R. Rahimipour), mmfarvizi@yahoo.com (M. Farvizi)

Please cite this article as: M. Abaei, M. R. Rahimipour, M. Farvizi, M. J. Eshraghi, Microstructure and Corrosion Behavior of Al-Cu-Fe Quasi-crystalline Coated Ti-6Al-4V Alloy, ***International Journal of Engineering, Transactions A: Basics***, Vol. 36, No. 10, (2023), 1880-1891

Velocity Oxygen Fuel (HVOF) are widely used to make quasicrystalline coatings, but these methods are associated with problems such as porosity, unmelted particles, cracks, and oxides [5, 6].

Magnetron sputtering is a widely used method for deposition wear and corrosion-resistant coatings. This method is economic and can be applied on samples with complex shapes. The quasi-crystalline phase formation depends on the substrate temperature [7, 8]. As experimentally shown, the substrate temperature should be higher than 500°C to obtain a single-phase quasicrystalline coating. The deposition of QCs on the substrates at room temperature leads to the evolution of the semicrystalline phase after subsequent heat treatment. The advantages of this method are high spraying speed at low operating voltages (700-800 V), low working gas pressure, low degree of pollution of the resulting film, and the possibility of obtaining uniform film thickness. However, the adjustment of stoichiometry in QCs is the main challenge [9-12].

Al-Cu-Fe-based quasicrystalline thin films show exceptional surface and mechanical properties. The direct growth of quasicrystals was reported in multilayer Al-Cu-Fe thin films after subsequent heat treatment [13]. Successful application of $Al_{60}Cu_{28}Fe_{12}$ quasicrystalline and film coating obtained through three-electrode ion-plasma sputtering of assembled targets was reported, and this coating contained a quasi-crystalline i-phase that was stable up to 723K [14]. The formation of the $Al_{62.5}Cu_{25}Fe_{12.5}$ quasicrystalline phase was achieved by the Al-Cu system at temperatures relatively higher than 500 (T>500°C). It is important to know that there are seven various compounds (Al_2Cu, Al_4Cu_9, AlCu, Al_xCu, Al_6Fe, Al_7Cu_2Fe, and $Al_{10}Cu_{10}Fe$) in the phase formation sequence before the icosahedron phase [15]. There was an increase in the amount and grain size of the i-phase throughout the process of annealing [16]. Phases that have a polyhedral atomic substructure in QCs, have greater nucleation rates within the system [17].

Uniaxial hot pressing was used to fabricate targets in the magnetron sputtering deposition process. The creation of cracks within the targets throughout film deposition can lead to statistical deviations in the coating composition when the AlCuFeB coating is applied in this way [7].

The Al–Cu–Fe QCs reveal high corrosion resistance and good hydrogen storage for use in catalytic reactions. These alloys, at low temperatures, have similar thermal properties to zirconia oxides, which are considered excellent insulators [18]. The investigation of corrosion resistance of AlCuFe thin film in NaCl solution approved its excellent performance [19]. The Corrosion behavior investigation of the quasicrystalline $Al_{63}Cu_{25}Fe_{12}$ alloy in a 5 % sodium chloride solution confirms the formation of a stable quasicrystalline icosahedral (ψ) phase [20]. According to corrosion experiments performed for 1, 2, 3, 4, and 8 days using 5% NaCl solution at 293 K, the Al-Cu-Fe films showed excellent corrosion resistance [21].

The limitations of titanium alloys, such as easy oxidation, and simple reaction with other materials can be overcome by adding Al and Cu to Ti. This procedure leads to the formation of significantly stable intermetallic metallurgical bonds and consequently, increases corrosion resistance. The Al-Cu-Ti combination is comparable to some icosahedrons like Al-Cu-Fe, which perform efficiently in surface engineering, as well as composite production [22, 23].

In the latest studies, icosahedral quasicrystals [24, 25], and characterization of thin films on the Ti6Al4V alloy substrate have been reported [26-29]. Als, in recent years, magnetron sputtering has received great attention for developing thin films [30].

Due to the above-mentioned problems of titanium alloys, and considering the necessity of applying an appropriate coating to improve the performance of titanium alloys, in this study, after the preparation of $Al_{62.5}Cu_{25}Fe_{12.5}$ quasi-crystalline powder mixture and appropriate target, the magnetron sputtering method was employed to deposit the QC coating on Ti-6Al-4V substrate. The microstructural aspects and electrochemical behavior of the substrate and the coated sample were studied and compared.

2. EXPERIMENTAL DETAILS

2. 1. Materials and Substrate Specifications Aluminum, iron, and copper powders with a purity of 99.9% were weighed using a scale with the precision of 0.0001 g in appropriate proportions to reach $Al_{62.5}Cu_{25}Fe_{12.5}$ composition. The substrate of the desired alloy was cut to 1 cm × 1 cm × 1 cm dimensions. The Spark Emission Spectroscopy test was used to investigate the alloy's chemical composition, the results of which are reported in Figure 1.

2. 2. Target Preparation Method The powder mixture was milled using a planetary ball-mill. The ball-to-powder weight ratio of 5:1 and a rotation speed of 220 rpm for 3 h were considered. After drying, the powders were compressed into discs having a 70 mm diameter and a 4 mm thickness in a uniaxial hydraulic press.

2. 3. Thin Film Preparation Before the coating deposition, the surfaces of the samples were sanded, degreased, and washed. Deposition of Al-Cu-Fe thin films on Ti6Al4V alloy substrates was carried out within a magnetic sputtering chamber, which had a 10^{-4} mbar base pressure. The deposition was accomplished at a pressure of 2.5×10^{-3} mbar under Argon gas (purity 99.998%) and at room temperature. A sputtering deposition technique using an AlCuFe ternary target with

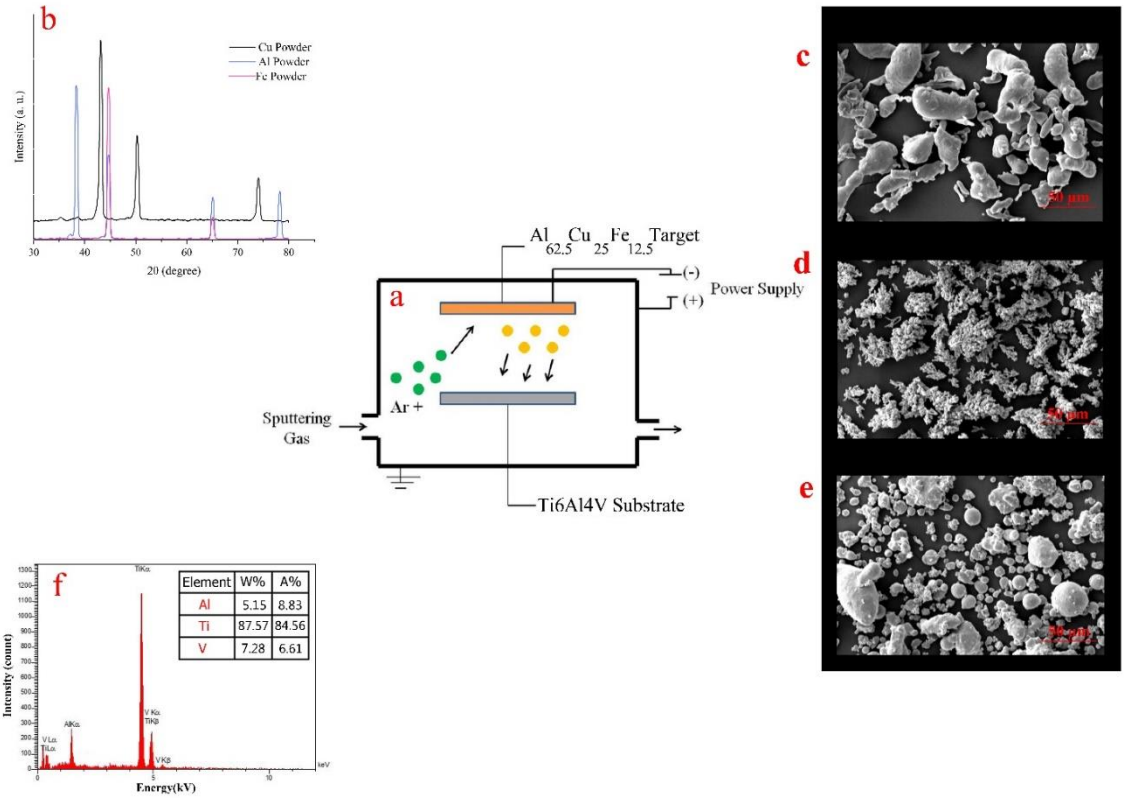

Figure 1. a) Schematic of the Magnetron Sputtering process: b) XRD results of primary powders, the morphology of the primary powders: c) Al, d) Cu, e) Fe, f) chemical composition of Ti6Al4V alloy

a composition of $Al_{62.5}Cu_{25}Fe_{12.5}$ was used to deposit the film. Figure 1 illustrates a schematic of the magnetron sputtering process. After the sputtering process, the samples were annealed with a continuous flow of 95% Argon and 5% H_2 at 700°C for 2 h [9, 10].

2. 4. Analysis Methods After annealing, the X-ray diffraction of the coated samples was performed by the Grazing-XRD method (XRD Philips PW1730 model) with the specifications of the 2.2 KW X-ray lamp. The identification of phases was done using Xpert HighScore software. The XRD method (Siemens, D500 system) with Cu K_α radiation at a 30-kV accelerating voltage was used to characterize the crystalline phases of different powders. SEM (VEGA II SCAN) and FESEM (Mira3 TESCAN model) were used to study the samples' microstructure. The EDS method was also employed to determine the chemical composition of the formed phases. A 3.5 wt% NaCl solution was considered to perform electrochemical measurements on the Ti6Al4V and AlCuFe samples (QC coated). The potentiodynamic polarization curves were examined to analyze the corrosion behavior. Model Prinston Applied Science EG&G parsta 2273 equipment was used for the electrochemical analysis. The standard corrosion test was used STM G59- 97 conducting potentiodynamic polarization resistance measurements.

3. RESULTS AND DISCUSSION

3. 1. $Al_{62.5}Cu_{25}Fe_{12.5}$ Powder Composition Figure 2 shows the morphology of $Al_{62.5}Cu_{25}Fe_{12.5}$ powder mixture after 3 h of mixing before and after heat treatment at 700°C for 2 h. The comparison of the morphology of starting powders including aluminum, copper, and iron powders (Figure 1(c), (d) and (e)) with those after mixing (Figure 2(a)) revealed that the morphology of the primary powders transformed into laminar shapes. Also, as can be seen in Figure 2(b), heat treatment of the powder mixture changes the morphology and leads to the evolution of the polyhedral particles in the mixture.

The elemental distribution map of $Al_{62.5}Cu_{25}Fe_{12.5}$ powder composition before and after annealing were shown in Figure 3. The presence of aluminum, copper, and iron elements in the distribution of elements indicate the AlCuFe mixing composition.

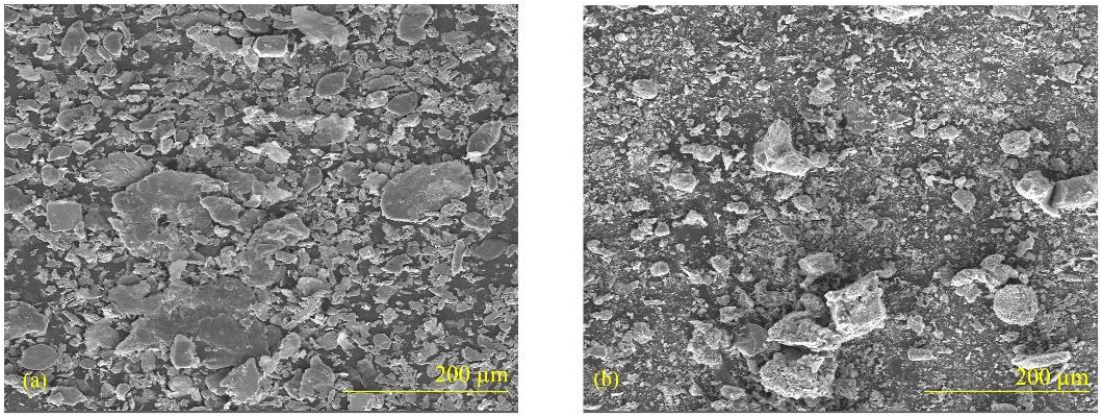

Figure 2. a) Morphology of $Al_{62.5}Cu_{25}Fe_{12.5}$ powder composition after 3 h of mixing, b) Morphology of $Al_{62.5}Cu_{25}Fe_{12.5}$ powder composition after heat treatment at 700°C for 2 h

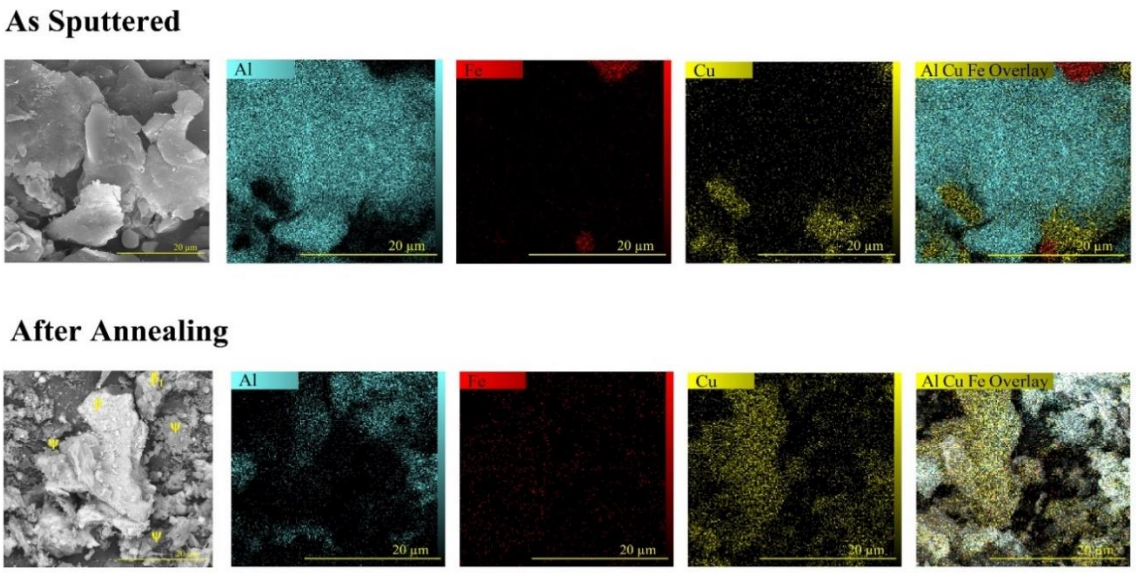

Figure 3. Elemental distribution map of $Al_{62.5}Cu_{25}Fe_{12.5}$ powder composition before and after annealing

Figures 4 shows the XRD results of the $Al_{62.5}Cu_{25}Fe_{12.5}$ powder mixture after 3 h of mixing before and after heat treatment at 700°C for 2 h.

The XRD pattern of the powder mixture before heat treatment confirmed that aluminum, copper, and iron powders were present and no new phase or solid solution appeared. The XRD pattern of the annealed powder mixture demonstrated the presence of Cu_3Al (β), and $AlFe_3$ (β_1) phases, as well as the quasi-crystalline ternary phase of $Al_{65}Cu_{20}Fe_{15}$ (ψ). The evolution of thepost-annealing quasi-crystalline phase of $Al_{65}Cu_{20}Fe_{15}$ has also been reported in other studies [31, 32]. Crystal structures and stable phases of Al-Cu-Fe ternary mechanisms were listed in Table 1.

3. 2. AlCuFe Thin Film Figure 5 shows the cross-section and the elemental distribution map taken from the cross-section of AlCuFe coating. The current thickness of the AlCuFe thin film was about 800 nm. No cracks or breaks were observed in the target during 135 min of sputtering due to the appropriate preparation of the target by mixing method, eventually leading to the formation of an AlCuFe thin film. The cross-section image in Figure 5 is displayed in the backscattered electrons (BSE) mode, accordingly indicating the area related to the thin film is brighter than the substrate.

Similar studies have reported a thickness of 85-260 nm for Al-Cu-Fe and Al-Co-Cu thin films accumulated on sodium chloride or glass, and ceramic substrates with three-electrode plasma [33]. Also, Al-Cu-Fe and Al-Cu-Fe-Sc quasi-crystalline films with 200 to 260 nm thicknesses have been obtained by ion-plasma sputtering of three electrodes [34]

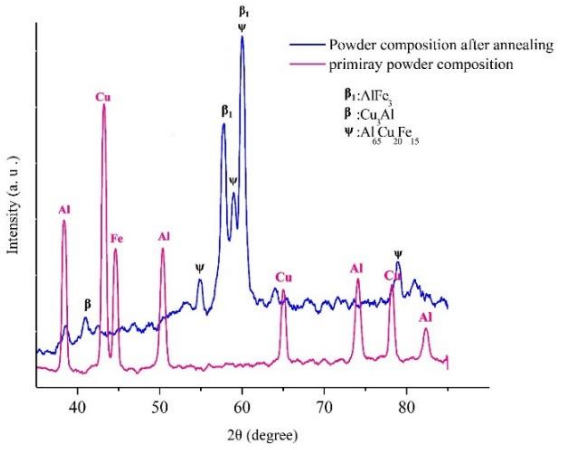

Figure 4. XRD patterns of AlCuFe powder mixture before and after heat treatment

The distribution of titanium and vanadium elements and Al, Cu, and Fe emphasized forming AlCuFe coating on the Ti-6Al-4V alloy as the substrate. As noted, there was neither Cu nor Fe in the substrate areas, and gradients were increasing for Cu and Fe and decreasing towards the thin film areas for Ti and V. Similarly, the very high catalytic performance of this alloy for methanol steam reforming was proven using the distribution map of aluminum, copper, iron, and oxygen elements of AlCuFe quasi-crystalline coating [35].

In another research, AlCuFe coating was deposited by the electron beam method. The study reported the microstructure of the coating in the cross-section and the distribution of chemical elements of aluminum, copper, and iron compared to the thickness of the coating. The results confirmed a relatively uniform distribution of elements along the cross-section of the coating [36].

Figures 6 shows the morphology of $Al_{62.5}Cu_{25}Fe_{12.5}$ thin film before and after heat treatment at 700°C for 2 h. The surface of the coating is completely continuous and without any visible cracks in two modes, as sputtered and after annealing. In the higher magnification, the morphological changes and multifaceted shapes are

TABLE 1. Crystal structures and stable phases of Al-Cu-Fe ternary mechanisms

Phase	Ideal formula	Present research	References Code	Structure	Other Researches
β_1	$AlFe_3$	Figure 3	00-050-0955	Body-centered cubic	[25]
β	Cu_3Al		00-028-0005		[24]
ψ	$Al_{65}Cu_{20}Fe_{15}$		00-042-1043	Quasicrystal	[17]

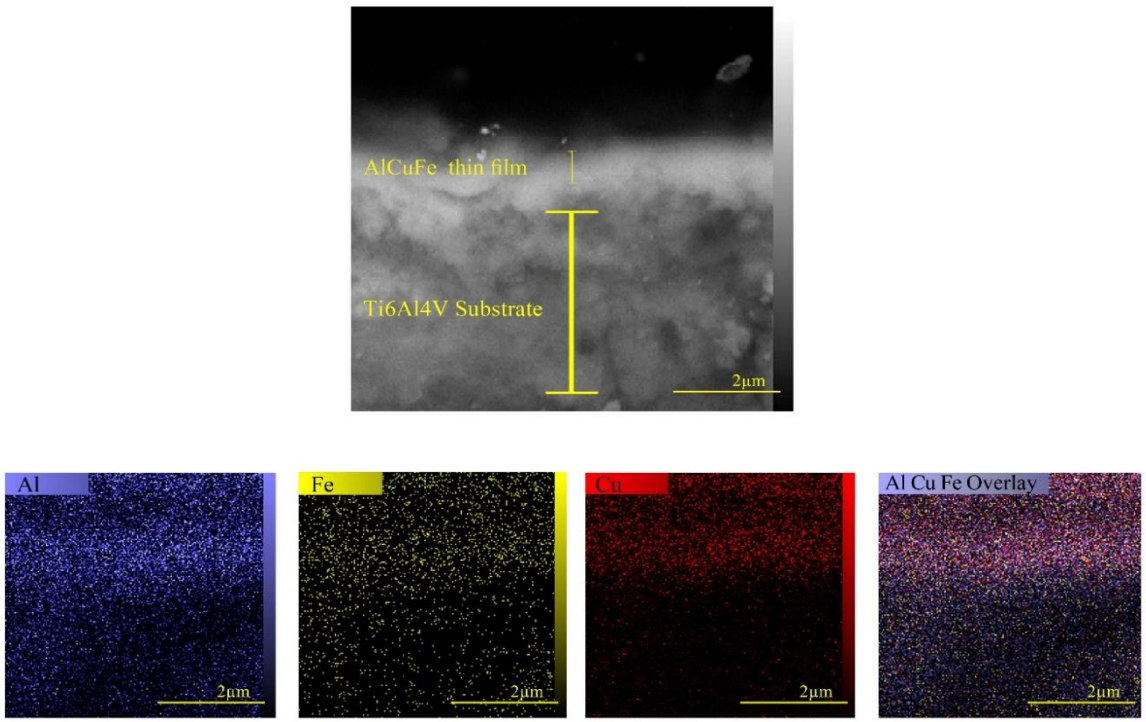

Figure 5. Cross section and distribution of cross-sectional elements of as sputtered AlCuFe coating applied on Ti-6Al-4V substrate

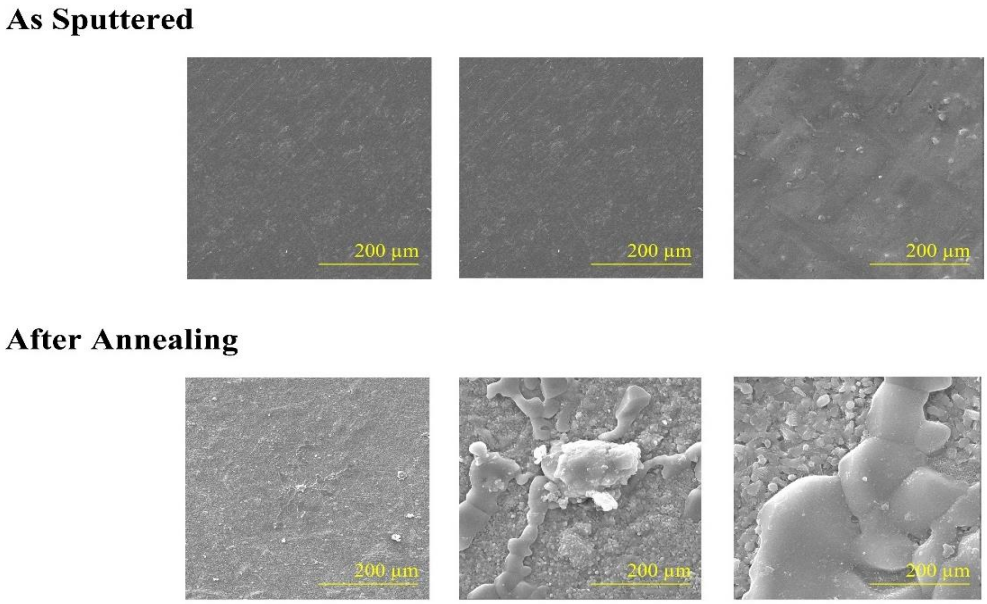

Figure 6. Morphology of AlCuFe coating applied on Ti-6Al-4V substrate before and after heat treatment at 700°C for 2 h

visible. Also, the five-facet morphology, which represents the presence of quasicrystal, is visible in the annealed thin film morphology. Figure 7 shows the distribution map of AlCuFe coating elements applied on the Ti-6Al-4V alloy substrate before and after annealing. As indicated in as sputtered thin film (before annealing), aluminum, copper, and iron elements had an even regional distribution on the coating surface. The identical distribution of aluminum, copper, and iron elements on the surface of the coating corroborates the AlCuFe coating formation. On the other hand, the distribution map of titanium element confirmed the entity of Ti-6Al-4V alloy substrate.

In the map images AlCuFe thin film after annealing, there are some areas empty of titanium, which indicates the creation of a coating on the substrate.

Figure 8 reports the XRD results of as-sputtered AlCuFe coating applied on Ti-6Al-4V after annealing. The XRD pattern of the AlCuFe coating shows the presence of Al_3Fe, and $AlTi_2$ phases, as well as the quasi-crystalline ternary phase of $Al_{65}Cu_{20}Fe_{15}$. The quasi-crystalline phase of $Al_{65}Cu_{20}Fe_{15}$ after annealing is reported in similar studies [1, 37]. According to the XRD analysis of the powders (Figure 4), the quasi-crystalline phase ψ was also visible in the AlCuFe thin film after annealing.

According to distribution map (Figure 7) the light areas were Cu- rich and Fe-rich, indicating ψ-phase whereas the other ones were Ti-rich revealing the $AlTi_2$ phase, in agreement with the phases detected by XRD (Figure 8).

The EDS results of the as-sputtered AlCuFe coating applied on the Ti-6Al-4V substrate are shown in Figure 9. The atomic percentages of aluminum, copper, and iron elements of the coating were 40.61, 9.23, and 22.71, respectively. The amount of aluminum in the coating (40.61 atomic percent) was lower than the amount of aluminum in the initial mixture (62.5 atomic percent), caused by the low deposition rate of aluminum. On the other hand, the high deposition rate led to a high amount of copper in the coating compared to the initial powder mixture.

Figure 10 shows the EDS results of the AlCuFe coating applied on the Ti-6Al-4V substrate by magnetic sputtering after heat treatment. Comparing the EDS results of the coating before annealing (Figure 9) and after annealing (Figure 10), the atomic percentage of the coating elements did not change significantly. According to Figure 10(b), the atomic percentage of aluminum, copper, and iron have been measured to be 41.15, 21.28, and 7.79, respectively, and the amount of titanium in the substrate is 29.78 atomic percent. The XRD (Figure 8) and EDS results (Figure 10(b)) confirmed the presence of the Al_3Fe and $AlTi_2$ phases. As can see in Figure10c, the EDS results related to ψ area show values of 59.25, 10.64, and 20.58 atomic percentages for aluminum, copper, and iron elements, respectively, which are very close to the EDS results of as sputtered thin film (Figure 9).

According to the EDS results from Figure 10(c) and the XRD results (Figure 8), this area indicates the presence of compounds with the stoichiometry of the initial powder ($Al_{62.5}Cu_{25}Fe_{12.5}$). It is also related to the formation of the $Al_{65}Cu_{20}Fe_{15}$ quasi-crystalline phase (ψ).

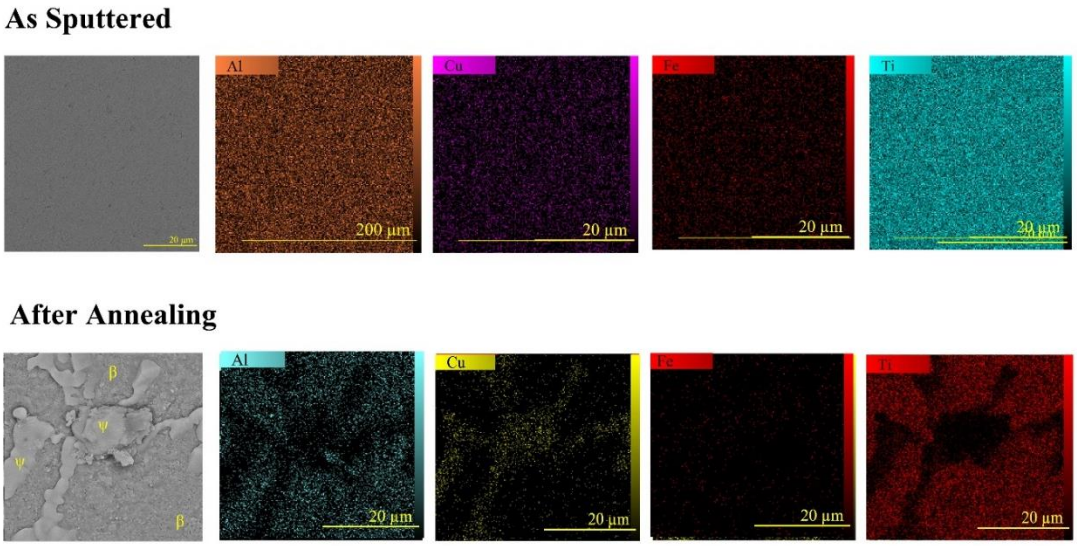

Figure 7. Elemental distribution map of AlCuFe coating applied on Ti-6Al-4V substrate before and after heat treatment

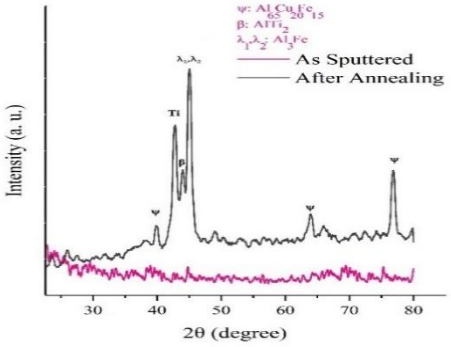

Figure 8. XRD results in AlCuFe coating applied on Ti-6Al-4V as sputtered and after annealing

3. 3. Investigating the Corrosion Properties of AlCuFe Thin Film Figure 11 displays the Nyquist curves (Z' in terms of -Z") of Ti-6Al-4V alloy (substrate) and Al-Cu-Fe thin film after annealing. In these curves, the increase in diameter demonstrates an increase in the corrosion resistance of the system. Therefore, it is clear from the shape of the Nyquist curves that the diameter of the curve in the substrate sample (Ti-6Al-4V alloy) is significantly greater than that of the Al-Cu-Fe thin film after annealing. The corresponding Bode-modulus impedance and Bode-phase angle curves of Ti-6Al-4V alloy (substrate) and Al-Cu-Fe thin film after annealing are shown in Figure 12. As indicated in Figure 12(a), the

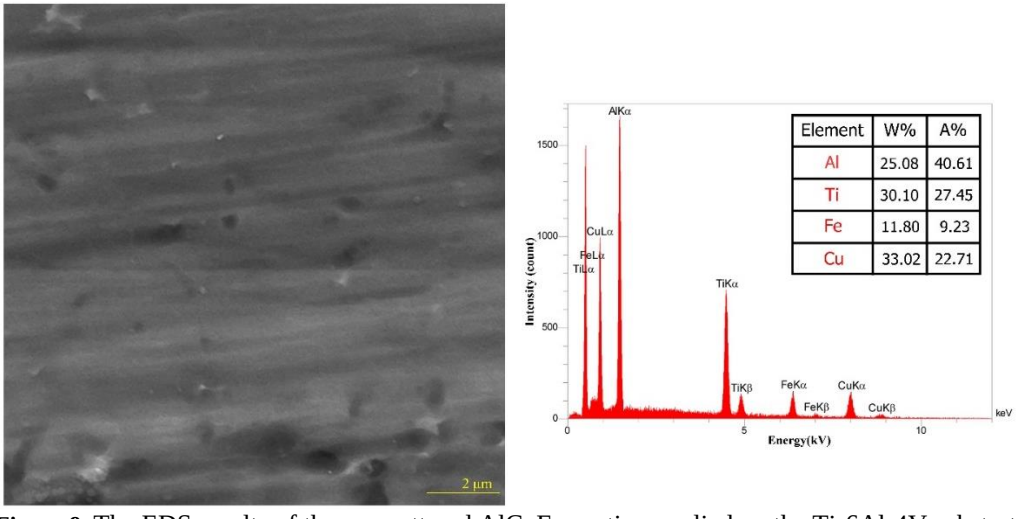

Figure 9. The EDS results of the as-sputtered AlCuFe coating applied on the Ti-6Al-4V substrate

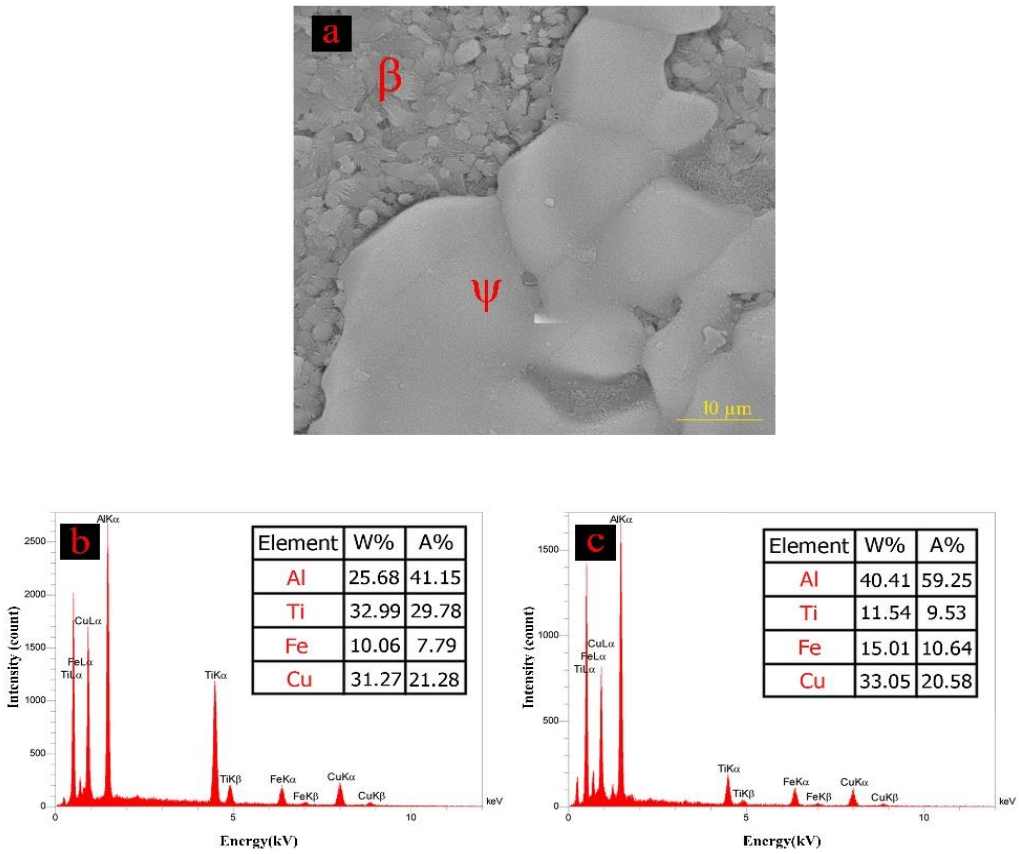

Figure 10. a) EDS results of the AlCuFe coating applied on the Ti-6Al-4V substrate after treatment, b) EDS results related to β areas, c) EDS results related to ψ area

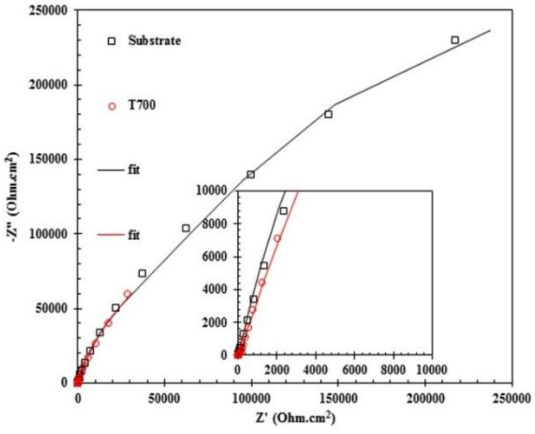

Figure 11. Nyquist diagrams in 3.5% NaCl solution at 25 °C for the selected samples in the form of Ti-6Al-4V alloy (substrate) and Al-Cu-Fe thin film after annealing (points of test results and the lines are the results of the fit)

impedance at the lowest frequency of the substrate was higher than the annealed Al-Cu-Fe thin film. Also, it is possible to obtain information about the anti-corrosion properties of the system from the Bode-phase angle diagrams. This evidence shows that the higher the phase angle value, the greater the resistance to electrolyte penetration [38]. Accordingly, it is obvious in the graphs of Figure 12(b) that the phase angle for the Ti-6Al-4V alloy (substrate) was higher in most frequencies compared to the Al-Cu-Fe thin film after annealing.

The impedance test results were matched on the electrochemical equivalent circuit of Figure 13 to more accurately determine the electrochemical parameters. The equivalent circuit shown in Figure 13 has three resistances (from the left, solution, coating, and charge transfer resistance) and two fixed phase elements (related to coating and double layer). This equivalent circuit is used when there is a coating on the surface, but the electrolyte has passed through the coating and reached the metal surface. Therefore there are two contact points between the electrolyte and the sample, including one between the electrolyte and the coating and another between the electrolyte and the metal surface. Therefore, the equivalent circuit of two-time constants is used. Ti-6Al-4V alloy (substrate) and Al-Cu-Fe thin film after annealing show an acceptable match with this equivalent circuit.

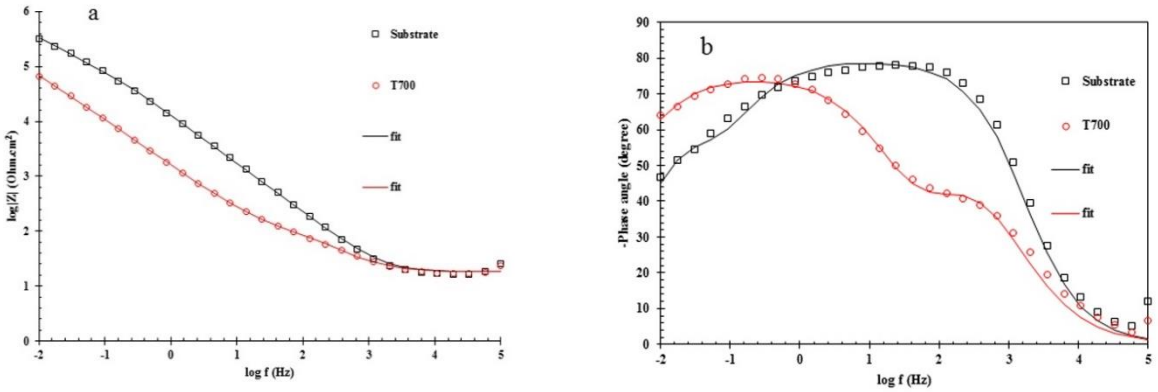

Figure 12. (a), Bode modulus diagrams (b), and Bode phase angle plots in 3.5% NaCl solution at 25 °C for the selected samples in the form of Ti-6Al-4V alloy (substrate) and Al-Cu-Fe thin film after annealing (points are test results and the lines are the results of the fit)

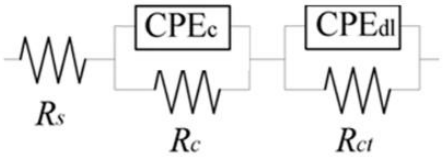

Figure 13. Electrochemical equivalent circuit of two-time constants used to model the results of the electrochemical impedance test

As can be seen, the modeling could match the Nyquist and Bud diagrams well, indicating the modeling results' reliability. The parameter values obtained from this modeling are reported in Table 2. According to Table 2, the substrate sample has a much higher total resistance than the substrate; thus, from the results of the electrochemical impedance test, it can be concluded that the substrate sample (Ti6Al4V alloy) was the optimal sample with the highest corrosion resistance value. It is

TABLE 2. Estimated values of the equivalent electric circuits of the Ti-6Al-4V alloy (substrate) and Al-Cu-Fe thin film after)

Sample	R_s (ohm.cm^2)	$Y0_c$ (S.sec^n .cm^{-2})	n_1	R_c (ohm.cm^2)	$Y0_{dl}$ (S.s^n .cm^{-2})	n_2	R_{ct} (ohm.cm^2)	R_t (ohm.cm^2)
Substrate	18.00	3.15E^{-05}	0.89	6.01E^5	2.86E^{-05}	0.88	5.43E^{+04}	6.55E^{+05}
T700	17.96	8.74E^{-05}	0.78	70.3	1.36E^{-04}	0.83	3.13E^{+05}	3.13E^{+05}

suggested to use higher annealing temperatures to achieve a quasi-crystalline structure with higher corrosion properties. Adding a fourth element such as chromium to the target is also suggested to attain the extraordinary corrosion properties of the quasi-crystalline coating. The polarization curves of the annealed coating and the substrate are shown in Figure 14. Data related to the current density and corrosion potential of the annealed coating and the substrate are reported in Table 3. Based on the polarization test results the annealed coating at 700°C showed a nobler behavior than the substrate (Ti-6Al-4V alloy). The data resulting from the calculations resulting from fitting the tangent to the cathodic and anodic branches are also positive (Table 3). Also, the coating annealed at 700 has become nobler by about 300 mV compared to the substrate, but its exchange current density remains almost close to the substrate. In a similar study evaluation of corrosion resistance of Bi-layered plasma-sprayed coating on titanium implants was investigated [39].

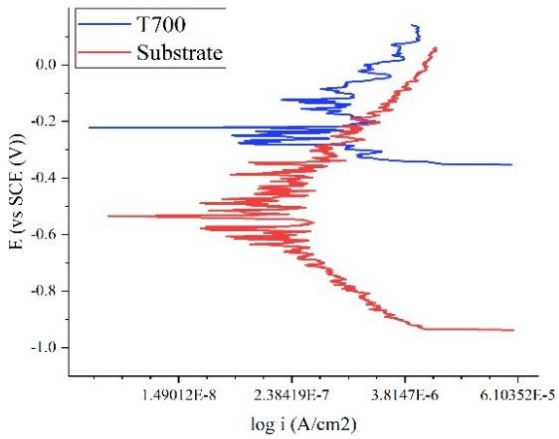

Figure 14. Polarization curves of annealed coating and substrate

TABLE 3. Current density and corrosion potential of annealed coating and substrate

Sample	E corr (mV)	i corr (A/cm^2)
Substrate	-0.54	$1.31*10^{-7}$
T700	-.022	$1.25*10^{-7}$

4. CONCLUSION

The following conclusions are summarized below:
1) After 3 h of mixing, the primary aluminum, copper, and iron powders were well mixed, and the mixed powders with $Al_{62.5}Cu_{25}Fe_{12.5}$ composition were prepared for the target of the magnetic sputtering process.
2) A thin layer of AlCuFe alloy free from cracks and discontinuities was coated on the Ti-6Al-4V substrate with an approximate thickness of 800 nm.
3) According to the distribution map of the AlCuFe coating elements applied on the Ti-6Al-4V alloy substrate, aluminum, copper, and iron elements' uniform distribution on the coating surface indicates post-annealing coating stability. There were no cracks, separations, or heterogeneous distribution in the map of the coating elements and surface morphology distribution.
4) XRD patterns related to the annealed powders and coating after heat treatment indicate the presence of Cu_3Al, $AlFe_3$, and quasi-crystalline ternary phases of $Al_{65}Cu_{20}Fe_{15}$ and Al_3Fe, $AlTi_2$, and $Al_{65}Cu_{20}Fe_{15}$ phases, respectively
5) Based on the polarization test results, the annealed coating at 700°C showed a better electrochemical behavior than the substrate (Ti-6Al-4V alloy).

5. REFERENCES

1. Gupta, M. K. , Etri, H.E., Korkmaz, M.E. , Ross, N.S., Krolczyk, G.M., Gawlik, J., Yaşar, N., and Pimenov, D.Y. "Tribological and surface morphological characteristics of titanium alloys: a review", ***Archives of Civil and Mechanical Engineering***, Vol. 22, No. 72, (2022), doi:10.1007/s43452-022-00392-x.
2. Fatoba, O., Akinlabi, S., Akinlabi, E. and Gharehbaghi, R., "Microstructural analysis, micro-hardness and wear resistance properties of quasicrystalline Al-Cu-Fe coatings on Ti-6Al-4V alloy", ***Materials Research Express***, Vol. 5, No. 6, (2018), 066538. doi: 10.1088/2053-1591/aaca70.
3. Litynska-Dobrzyńska, L., Stan-Glowinska, K., Wójcik, A., Duraczyńska, D., and Serwicka, E.M., "Microstructure and catalytic activity of melt-spun Al-Cu-Fe ribbons", ***Materials Science Forum***, Vol. 985, (2020), 109-114. 10.4028/www.scientific.net/MSF.985.109.
4. Mishra, S., Yadav, T., Singh, S., Singh, A., Shaz, M., Mukhopadhyay, N., and Srivastava, O.N., "Evolution of porous structure on Al-Cu-Fe quasicrystalline alloy surface and its catalytic activities", ***Journal of Alloys and Compounds***, Vol. 834, (2020), 155-162. https://doi.org/10.1016/j.jallcom.2020.155162.
5. Parsamehr, H., Chen, T.-S., Wang, D.-S., Leu, M.-S., Han, I., Xi, Z., Tsai, A.-P., Shahani, A.J. and Lai, C.-H., "Thermal spray coating of Al-Cu-Fe quasicrystals: Dynamic observations and surface properties", ***Materialia***, Vol. 8, (2019), 100432. doi: 10.1016/j.mtla.2019.100432.
6. Mora, J., García, P., Muelas, R. and Agüero, A., "Hard quasicrystalline coatings deposited by HVOF thermal spray to reduce ice accretion in aero-structures components", ***Coatings***, Vol. 10, No. 3, (2020), 290. doi: https://doi.org/10.3390/coatings10030290.
7. Shaĭtura, D. and Enaleeva, A.J., "Fabrication of quasicrystalline coatings: A review", ***Crystallography Reports***, Vol. 52, No. 6, (2007). doi: https://doi.org/10.1134/S1063774507060041.
8. Widjaja, E.J., and Marks, L.J., "In situ studies of magnetron sputtered Al–Cu–Fe–Cr quasicrystalline thin films", ***Thin Solid Films***, Vol. 420, (2002), 295-299. https://doi.org/10.1016/S0040-6090(02)00809-X.
9. Parsamehr, H., Lu, Y.-J., Lin, T.-Y., Tsai, A.-P. and Lai, C.H., "In-situ observation of local atomic structure of Al-Cu-Fe quasicrystal formation", ***Scientific Reports***, Vol. 9, No. 1, (2019), 1245. doi: https://doi.org/10.1038/s41598-018-37644-x.
10. Parsamehr, H., Yang, C.-L., Liu, W.-T., Chen, S.-W., Chang, S.-Y., Chen, L.-J., Tsai, A.P. and Lai, C.-H., "Direct observation of growth and stability of Al-Cu-Fe quasicrystal thin films", ***Acta Materialia***, Vol. 174, (2019), 1-8. https://doi.org/10.1016/j.actamat.2019.05.024.
11. Parsamehr, H., Chang, S.Y., and Lai, C.H., "Mechanical and surface properties of aluminum-copper-iron quasicrystal thin films", ***Journal of Alloys and Compounds***, Vol. 732, (2018), 952-957. https://doi.org/10.1016/j.jallcom.2017.10.229.
12. Widjaja, E.J and Marks, L.D, "Microstructural evolution in Al–Cu–Fe quasicrystalline thin films", ***Thin Solid Films***, Vol. 441, No. 1-2, (2003), 63-71. https://doi.org/10.1016/S0040-6090(03)00903-9.
13. Olsson, S., Eriksson, F., Birch, J. and Hultman, L., "Formation of α-approximant and quasicrystalline Al-Cu-Fe thin films", ***Thin Solid Films***, Vol. 526, (2012), 74-80. doi: https://doi.org/10.1016/j.tsf.2012.11.009.
14. Ryabtsev, S., Polonskyi, V. and Sukhova, O.V., "Structure and corrosion of quasicrystalline cast alloys and Al-Cu-Fe film coatings", ***Materials Science***, Vol. 56, No. 2, (2020), 263-272. doi: 10.1007/s11003-020-00428-8.
15. Haidara, F., Duployer, B., Mangelinck, D., and Record, M.C., "In-situ investigation of the icosahedral Al–Cu–Fe phase formation in thin films", ***Journal of Alloys and Compounds***, Vol. 534, (2012), 47-51. doi: https://doi.org/10.1016/j.jallcom.2012.04.036.
16. Lee, K., Chen, Y., Dai, W., Naugle, D., and Liang, H., "Design of quasicrystal alloys with favorable tribological performance given microstructure and mechanical properties", ***Materials and Design***, Vol. 193, (2020), 108735. https://doi.org/10.1016/j.matdes.2020.108735.
17. Wolf, W., Kube, S.A., Sohn, S., Xie, Y., Cha, J.J., Scanley, B.E., Kiminami, C.S., Bolfarini, C., Botta, W.J. and Schroers, J., "Formation and stability of complex metallic phases including quasicrystals explored through combinatorial methods", ***Scientific Reports***, Vol. 9, No. 1, (2019), 1-11. https://doi.org/10.1038/s41598-019-43666-w.
18. Jamshidi Rodbari, R. and Agostinho Jamshi, L.C.L, "Evolution of the phases of quasicrystalline alloys icosahedral/decagonal $Al_{62.2}Cu_{25.3}Fe_{12.5}/Al_{65}Ni_{15}Co_{20}$ and oxidative behavior", ***Journal of the Chilean Chemical***

Society, Vol. 63, No. 2, (2018), 3928–3933. doi: 10.4067/s0717-97072018000203928.

19. Babilas, R., Bajorek, A., Spilka, M., Radoń, A., and Łoński, W., "Structure and corrosion resistance of Al–Cu–Fe alloys", ***Progress in Natural Science: Materials International***, Vol. 30, No. 3, (2020), 393-401. doi: https://doi.org/10.1016/j.pnsc.2020.06.002.
20. Sukhova, O., and Polonskyy, V., "Peculiarities in structure formation and corrosion of cast quasicrystalline $Al_{63}Cu_{25}Fe_{12}$ and $Al_{63}Co_{24}Cu_{13}$ alloys in sodium chloride aqueous solution", ***Physics and Chemistry of Solid State***, Vol. 21, No. 3, (2020), 530-536. doi: https://doi.org/10.15330/pcss.21.3.530-536.
21. Ryabtsev, S.I, Sukhova, O.V, and Polonskyy, V.A., "Structure and corrosion in NaCl solution of quasicrystalline Al–Cu–Fe cast alloys and thin films", ***Journal of Physics and Electronics***,Vol. 27, No. 1, (2019), 27-30. doi: 10.15421/331904.
22. Liu, S., and Shin, Y.C., "Additive manufacturing of Ti6Al4V alloy: A review", ***Materials and Design***, Vol. 164, (2019), 107552. https://doi.org/10.1016/j.matdes.2018.107552.
23. Fatoba, O., Lasisi, A., Ikumapayi, O., Akinlabi, S. and Akinlabi, E., "Icosahedral structure influence on the microstructural and mechanical properties of laser additive manufactured (LAM) titanium alloy grade 5", ***Materials Today: Proceedings,*** Vol. 44, (2021), 1263-1270. doi:10.1016/j.matpr.2020.11.263.
24. Shukla, A.K., Ledieu, J., Gaudry, E., Wu, D.M., Lograsso, T.A., and Fournée, V., "Quantum size effects in Ag thin films grown on the fivefold surface of the icosahedral Al-Cu-Fe quasicrystal: Influence of the growth temperature", ***Journal of Vacuum Science and Technology A***, Vol. 40, (2022), 013212. Doi: https://doi.org/10.1116/6.0001450.
25. Singha, A., Hiroto, T., Odea, M., Takakurac, H., Tesarˇ, K., Somekawaa, H., and Hara, T., "Precipitation of stable icosahedral quasicrystal phase in a Mg-Zn-Al alloy", ***Acta Materialia***, Vol. 225, (2022), 117563. https://doi.org/10.1016/j.actamat.2021.117563.
26. Gashti, M., Mehdinavaz Aghdam, R., Motallebzadeh, A., Gharibi Asl, F., Soltani, R., Ashraf, A., Balaei, H., and Razazzadeh, A., "Bio-Corrosion, Mechanical and Microstructural Properties of TiTaMoVZr High-Entropy Alloy Film on Ti–6Al–4V Substrate", ***Metals and Materials International***, (2022), https://doi.org/10.1007/s12540-023-01464-0.
27. Phan, N.H., Donga, P.V., Muthuramalingam, T., Thiena, N.V., Dunga, H.T., Hunga, T.Q., Duca, N.V., and Lya, N.T., "Experimental Investigation of Uncoated Electrode and PVD AlCrNi Coating on Surface Roughness in Electrical Discharge Machining of Ti-6Al-4V", ***International Journal of Engineering, Transactions A: Basics,*** Vol. 34, No. 04, (2021), 928-934. Doi: 10.5829/ije.2021.34.04a.19.
28. Rahmouni, K., Besnard, A., Oulmi, K., Nouveau, C., Hidoussi, A., Aissani, L., and Zaabat, M., "In vitro corrosion response of CoCrMo and Ti-6Al-4V orthopedic implants with Zr columnar thin films ", ***Surface and Coatings Technology***, Vol. 436, (2022), 128310. https://doi.org/10.1016/j.surfcoat.2022.128310.
29. Tsai, S.Y., Chen, Y.A., You, J.D., Chu, J.P., and You, P., "Micro-scale tribological study of a Ni-Cr-Fe-Ti-Al-V high entropy alloy thin film by magnetron co-sputtering of Inconel-718 and Ti-6Al-4V ", ***Surface and Coatings Technology***, Vol. 464, (2023), 129481. https://doi.org/10.1016/j.surfcoat.2023.129481.
30. Nikravesh, M., Akbaria, G.H., and Poladi, A., Mechanical Properties and Microstructural Evolution of Ta/TaNx Double Layer Thin Films Deposited by Magnetron Sputtering, ***International Journal of Engineering, Transactions B: Applications,*** Vol. 30, No. 2, (2017) 288-293. doi: 10.5829/idosi.ije.2017.30.02b.16
31. Zhu, L., Soto-Medina, S., Cuadrado-Castillo, W., Hennig, R.G., and Manuel, M.V., "New experimental studies on the phase diagram of the Al-Cu-Fe quasicrystal-forming system", ***Materials and Design,*** Vol. 185, (2020), 108186. doi: https://doi.org/10.1016/j.matdes.2019.108186.
32. Huttunen-Saarivirta, E.J., "Microstructure, fabrication, and properties of quasicrystalline Al–Cu–Fe alloys: A review", ***Journal of Alloys and Compounds***, Vol. 363, No. 1-2, (2004), 154-178. https://doi.org/10.1016/S0925-8388(03)00445-6.
33. Ryabtsev, S. and Sukhova, O., "Ion-plasma deposition of thin quasicrystalline Al-Cu-Fe and Al-Cu-Co films", ***Problems of Atomic Science and Technology***, Vol. 126, No. 2, (2020), 126-145. doi: 10.46813/2020-126-145.
34. Ryabtsev, S., Polonskyy, V., and Sukhova, O., "Effect of scandium on the structure and corrosion properties of vapor-deposited nanostructured quasicrystalline Al–Cu–Fe films", ***Powder Metallurgy and Metal Ceramics***, Vol. 58, No. 9-10, (2020), 567-575. doi: 10.1007/s11106-020-00111-2
35. Kameoka, S., Tanabe, T., Satoh, F., Terauchi, M., and Tsai, A.P., "Activation of Al–Cu–Fe quasicrystalline surface: Fabrication of a fine nanocomposite layer with high catalytic performance", ***Science and Technology of Advanced Materials***, Vol. 15, No. 1, (2014). doi: 10.1088/1468-6996/15/1/014801.
36. Polishchuk, S., Ustinov, A., Telychko, V., Merstallinger, A., Mozdzen, G., and Melnichenko, T., "Fabrication of thick, crack-free quasicrystalline Al–Cu–Fe coatings by electron-beam deposition", ***Surface and Coatings Technology***, Vol. 291, (2016), 406-412. doi: 10.1016/j.surfcoat.2016.03.002.
37. Wang, X., Guan, R., Misra, R., Wang, Y., Li, H., Shang, Y, "The mechanistic contribution of nanosized Al_3Fe phase on the mechanical properties of Al-Fe alloy", ***Surface and Coatings Technology***, Vol. 724, (2018), 452-460. doi: 10.1016/j.msea.2018.04.002.
38. Mahdavian, M. and Attar, M., "Another approach in theanalysis of paint coatings with eis measurement: Phase angle at high frequencies", ***Corrosion Science***, Vol. 48, No. 12, (2006), 4152-4157. https://doi.org/10.1016/j.corsci.2006.03.012.
39. Ebrahimi, N., Sedaghat Ahangari Hosseinzadeh, A., Vaezi, M., and Mozafari, M., "Evaluation of Corrosion Resistance of Bi-layered Plasma-sprayed Coating on Titanium Implants", ***International Journal of Engineering, Transactions A: Basics,*** Vol. 35, No. 04, (2022) 635-643. doi: 10.5829/ije.2022.35.04A.03.

Persian Abstract

چکیده

آلیاژ Ti-6Al-4V اغلب در صنایع هوافضا، دریایی و خودرویی کاربرد دارد .علیرغم خواص عالی آلیاژTi-6Al-4V ، حساسیت بالا به خوردگی، پایداری حرارتی ضعیف و خواص تریبولوژیکی ضعیف کاربردهای آنها را محدود کرده است. در این تحقیق، ابتدا مخلوط پودری $Al_{62.5}Cu_{25}Fe_{12.5}$ آماده سازی گردید که این ترکیب در محدوده تشکیل فازهای شبه بلوری است. فیلم نازک Al-Cu-Fe با روش کندوپاش مگنترون بر روی زیرلایه Ti-6Al-4V با ضخامت ۸۰۰ نانومتر رسوب داده شد. لایه های نازک Al-Cu-Fe و ترکیب پودری در دمای ۷۰۰ درجه سانتیگراد به مدت ۲ ساعت آنیل شدند. تجزیه و تحلیل ریزساختار و مورفولوژی ترکیب پودری و پوشش‌های شبه کریستالی Al-Cu-Fe ایجاد شده بر روی آلیاژTi-6Al-4V با استفاده از آنالیز میکروسکوپ الکترونی روبشی (SEM) و تست XRD مورد بررسی قرار گرفت .اندازه‌گیری‌های الکتروشیمیایی در محلول ۳/۵ درصد NaCl انجام شد. نتایج نشان داد که لایه نازک آلیاژ Al-Cu-Fe بدون هیچ ترک بر روی سطح آلیاژ Ti-6Al-4V رسوب کرده است. الگوهای XRD مربوط به پودرهای آنیل شده نشان دهنده حضور فازهای Cu_3Al ، $AlFe_3$و فاز شبه بلوری $Al_{65}Cu_{20}Fe_{15}$ است. الگوهای XRD پوشش پس از عملیات حرارتی نشان دهنده حضور فازهای Al_3Fe ، $AlTi_2$ و فاز شبه بلوری $Al_{65}Cu_{20}Fe_{15}$ است که این فاز شبه بلوری در پودرهای آنیل شده نیز مشاهده گردید. بر اساس نتایج تست پلاریزاسیون، پوشش آنیل شده در دمای ۷۰۰ درجه سانتیگراد رفتار نجیب تری نسبت به زیرلایه (آلیاژ Ti-6Al-4V) نشان داد.